

El Niño–Southern Oscillation correlated aerosol Ångström exponent anomaly over the tropical Pacific discovered in satellite measurements

Jing Li,^{1,2} Barbara E. Carlson,¹ and Andrew A. Lacis²

Received 30 January 2011; revised 8 July 2011; accepted 18 July 2011; published 22 October 2011.

[1] El Niño–Southern Oscillation (ENSO) is the dominant mode of interannual variability in the tropical atmosphere. ENSO could potentially impact local and global aerosol properties through atmospheric circulation anomalies and teleconnections. By analyzing aerosol properties, including aerosol optical depth (AOD) and Ångström exponent (AE; often used as a qualitative indicator of aerosol particle size) from the Moderate Resolution Imaging Spectrometer, the Multiangle Imaging Spectroradiometer and the Sea-viewing Wide Field-of-view Sensor for the period 2000–2011, we find a strong correlation between the AE data and the multivariate ENSO index (MEI) over the tropical Pacific. Over the western tropical Pacific (WTP), AE increases during El Niño events and decreases during La Niña events, while the opposite is true over the eastern tropical Pacific (ETP). The difference between AE anomalies in the WTP and ETP has a higher correlation coefficient (>0.7) with the MEI than the individual time series and could be considered another type of ENSO index. As no significant ENSO correlation is found in AOD over the same region, the change in AE (and hence aerosol size) is likely to be associated with aerosol composition changes due to anomalous meteorological conditions induced by the ENSO. Several physical parameters or mechanisms that might be responsible for the correlation are discussed. Preliminary analysis indicates surface wind anomaly might be the major contributor, as it reduces sea-salt production and aerosol transport during El Niño events. Precipitation and cloud fraction are also found to be correlated with tropical Pacific AE. Possible mechanisms, including wet removal and cloud shielding effects, are considered. Variations in relative humidity, tropospheric ozone concentration, and ocean color during El Niño have been ruled out. Further investigation is needed to fully understand this AE-ENSO covariability and the underlying physical processes responsible for it.

Citation: Li, J., B. E. Carlson, and A. A. Lacis (2011), El Niño–Southern Oscillation correlated aerosol Ångström exponent anomaly over the tropical Pacific discovered in satellite measurements, *J. Geophys. Res.*, *116*, D20204, doi:10.1029/2011JD015733.

1. Introduction

[2] El Niño–Southern Oscillation (ENSO) is a coupled atmospheric-oceanic cycle in the tropical Pacific Ocean [Diaz *et al.*, 2001] and is the dominant mode of interannual variability of tropical climate. ENSO events, representing changes in tropical sea surface temperature and other geophysical parameters relative to average conditions, have been shown to significantly impact local and global climate and could potentially influence the emission and distribution of aerosols and trace gases [e.g., Chandra *et al.*, 1998,

2009a, 2009b; Ziemke and Chandra, 2003; Logan *et al.*, 2008; Podgorny *et al.*, 2003].

[3] The positive ENSO phase brings the warm sea surface temperature anomaly further east, suppresses convection over the west Pacific, and intensifies biomass burning over the Indonesian region [Chandra *et al.*, 1998, 2009b; Logan *et al.*, 2008]. van der Werf *et al.* [2006] showed a significant increase in CO emissions occurred owing to the enhanced fires in Indonesia during the 1997 El Niño. Similar but less dramatic increases in tropospheric CO, O₃ and a decrease in H₂O associated with the strong El Niño event of 2006 were reported by Logan *et al.* [2008]. Increases in fire activities during El Niño have also been found over the northern part of South America [Le Page *et al.*, 2007]. Increases in fires tend to produce more carbonaceous aerosols, which change aerosol optical properties and thus their radiative effects. In addition to biomass burning, Prospero and Lamb [2003] found that the Barbados dust concentration is enhanced by

¹Department of Earth and Environmental Sciences, Columbia University, New York, New York, USA.

²NASA Goddard Institute for Space Studies, New York, New York, USA.

warm ENSO events linked to droughts in west Africa. Australian dust emission may also be enhanced by the El Niño induced dry conditions [Mitchell *et al.*, 2009].

[4] During the cold ENSO (La Niña) phase, dynamical processes are largely reversed with respect to the warm phase. Also, Gong *et al.* [2006] indicated a positive correlation between central and eastern Asia dust emission and La Niña events through model simulations.

[5] While most of the above studies focus on trace gases or aerosol optical depth, ENSO-induced anomalies in biomass burning activities and dust emissions have the potential to alter aerosol composition and/or size distribution over the tropical region, which also play important roles in aerosol direct and indirect effects. Increasing biomass burning tends to produce more fine-mode aerosol particles that increase the AE, while increasing dust has the opposite effect by decreasing the AE. Moreover, aerosol transport pathways may also be shifted by atmospheric circulation anomalies.

[6] The Ångström exponent (AE) is used to parameterize the relationship between aerosol size and dependence of optical depth on wavelength:

$$\alpha = -\ln(\tau/\tau_1)/\ln(\lambda/\lambda_1) \quad (1)$$

where α is the AE parameter, and τ and τ_1 are aerosol optical depth at λ and λ_1 , respectively. In general, values of $\alpha \leq 1$ indicate size distributions dominated by coarse mode aerosols that are typically associated with dust and sea salt, and values of $\alpha \geq 2$ indicate size distributions dominated by fine mode aerosols that are usually associated with urban pollution and biomass burning [Eck *et al.*, 1999; Westphal and Toon, 1991]. Kaufman *et al.* [1994] demonstrated that the AE computed in the 0.44–1.03 μm range can be a good indicator of the fraction of small particles with radii $r = 0.057$ – $0.21 \mu\text{m}$ relative to larger particles with radii $r = 1.8$ – $4 \mu\text{m}$ for tropospheric aerosols. In this study, we investigate the interannual variability of the AE parameter over tropical Pacific using the MODIS, MISR and SeaWiFS satellite data sets. We demonstrate a covariability of the AE time series with the multivariate ENSO index (MEI). We find that monthly mean AE over the western tropical Pacific (WTP) tends to increase during El Niño events and decrease during La Niña events, while that over the eastern tropical Pacific (ETP) has the opposite behavior. The difference between WTP and ETP AE anomalies has stronger correlation with MEI than each individual time series and could serve as a new type of ENSO index. We also investigate possible physical processes that could lead to this AE-ENSO correlation using meteorological data, including aerosol emission changes over source regions, aerosol transport path changes with atmospheric circulation anomalies and cloud and precipitation pattern shifts over the tropical Pacific.

[7] Section 2 introduces difference satellite AE data sets used for the study. Section 3 presents major results and findings. Section 4 discusses possible mechanisms leading to the results. Also, a summary of the study is given in section 5.

2. Data Sets

2.1. Satellite AE Data

[8] In this study, we employ AE products from MODIS, MISR and SeaWiFS satellite sensors to investigate its

interannual variability and correlation with ENSO. We use the multisensor data sets to evaluate the robustness of the results. Analysis is focused on the MODIS data, with measurements from MISR and SeaWiFS providing independent corroboration of the MODIS results.

[9] The Moderate Resolution Imaging Spectroradiometer (MODIS) [Kaufman *et al.*, 1997; Tanré *et al.*, 1997] sensor was launched onboard EOS-Terra in December 1999 and later on EOS-Aqua in May 2002. We use the level 3 monthly mean AE products from Collection 005 [Levy *et al.*, 2007a, 2007b; Remer *et al.*, 2008] at $1^\circ \times 1^\circ$ resolution from both the Terra and Aqua platforms. The temporal coverage for Terra MODIS is July 2000 to March 2011, and October 2002 to March 2011 for Aqua MODIS. The first few months have been excluded because of some instability observed in the data. Different retrieval algorithms are used in processing the MODIS data over land and ocean and the AE product is reported using the 440/670 nm wavelength pair over land and the 550/865 nm wavelength pair over ocean [Remer *et al.*, 2005; Levy *et al.*, 2007a]. Note that the AE product is retrieved over water surface, but is model dependent in the over-land retrieval [Remer *et al.*, 2005; Levy *et al.*, 2010]. Validation of MODIS ocean aerosol products using surface measurements indicates that aerosol effective radius retrievals are accurate within $\pm 0.11 \mu\text{m}$ [Remer *et al.*, 2002; Levy *et al.*, 2005], whereas over land the quality of the AE is significantly lower and is not suitable for quantitative studies [Levy *et al.*, 2010]. Similarly, we have found that the agreement between MODIS and AERONET-retrieved AE is better over ocean stations than over land. Therefore, we primarily focus on the analysis of the ocean data.

[10] The Multiangle Imaging Spectroradiometer (MISR) [Diner *et al.*, 1998] was also launched onboard EOS-Terra satellite in December 1999. The instrument has a wider range of viewing angles compared to MODIS. The aerosol retrieval algorithm has been described in the work of Martonchik *et al.* [2009]. The MISR AE is calculated using a linear least squares fit to the logarithm of optical depth as a function of the logarithm of the four MISR wavelengths (446, 558, 672 and 866 nm). Here we use version F15_0031 Level 3 monthly averaged AE product from July 2000 to March 2011 (to be consistent with Terra MODIS). The data have been rescaled from the $0.5^\circ \times 0.5^\circ$ resolution to $1^\circ \times 1^\circ$. The rescaling is performed by assigning equal weight to each subgrid, and the final $1^\circ \times 1^\circ$ grid box is considered valid only when more than half of the subgrids have valid data.

[11] The Sea-viewing Wide Field-of-view Sensor (SeaWiFS) [Hooker *et al.*, 1992], launched on SeaStar in August 1997, provides multispectral retrievals of aerosol optical thickness and Ångström exponent over the ocean as by products of ocean color measurements [Gordon and Wang, 1994; Wang, 2000]. The SeaWiFS AE is reported at the 510/865 nm spectral interval. We use monthly mean Level 3 AE data from July 2000 to December 2010 to be consistent with Terra MODIS and MISR data time period. The data has been degraded from $1/12^\circ \times 1/12^\circ$ resolution to $1^\circ \times 1^\circ$ resolution using the same strategy as for the MISR data.

[12] In addition to the AE data, we use cloud fraction and cirrus reflectance from MODIS, column precipitation from Global Precipitation Climatology Project (GPCP) and the vertical feature mask data set from the Cloud-Aerosol Lidar and Infrared Pathfinder Satellite Observations (CALIPSO).

These correlative measurements are used to investigate the mechanisms responsible for the observed ENSO signal in the AE data.

2.2. ENSO Index and Meteorological Data

[13] In this study we use the monthly mean multivariate ENSO index from 2000 to 2011. The MEI is used to identify ENSO events on the basis of six main observed variables over the tropical Pacific, including sea-level pressure, zonal and meridional components of the surface wind, sea surface temperature, surface air temperature, and total cloudiness fraction of the sky. The MEI is calculated as the first unrotated principal component of all six observed fields combined. The numerical values can be found at <http://www.esrl.noaa.gov/psd/people/klaus.wolter/MEI/mei.html>.

[14] We also use sea surface temperature (SST), horizontal wind field, precipitation, relative humidity and cloud fraction to examine satellite-retrieved aerosol variability with ENSO. The SST data used is NOAA Optimum Interpolation SST data (NOAA_OI_SST_V2, available at <http://www.esrl.noaa.gov/psd/data/gridded/data.noaa.oisst.v2.html>; see Reynolds *et al.* [2002]) at $1^\circ \times 1^\circ$ resolution. Wind and relative humidity fields are from the National Centers for Environmental Prediction and National Center for Atmospheric Research (NCEP/NCAR) Reanalysis 2 Data (available from <http://www.esrl.noaa.gov/psd/>; see Kanamitsu *et al.* [2002]), with a horizontal resolution of $2.5^\circ \times 2.5^\circ$ and 17 pressure levels for wind and relative humidity. Precipitation data are from Global Precipitation Climatology Project (GPCP) [Adler *et al.*, 2003]. The horizontal resolution is also $2.5^\circ \times 2.5^\circ$. Cloud fraction product is from Terra MODIS C005 level 3 at $1^\circ \times 1^\circ$. All data are on a monthly mean basis and the time periods are matched to that of Terra MODIS AE.

3. Results

[15] Empirical orthogonal function (EOF) analysis [Bjornsson and Venegas, 1997] is an effective method to investigate the spatial and temporal variability of multidimensional data sets. It aims to objectively identify the major modes of space-time variability by decomposing the data matrix into a set of orthogonal eigenvectors. Here EOF analysis is performed on the AE data from the four satellite data sets after removing the mean season cycle over the tropical Pacific Ocean (10°S to 10°N , 100°E to 80°W).

[16] In the EOF results, we searched for the mode that has the highest correlation coefficient with the MEI time series that is acceptable (>0.5) at the 95% confidence level. According to this criterion, we find that the second EOF of MODIS and SeaWiFS and the dominant EOF of MISR AE, together with the corresponding PCs of space-time variability are highly correlated with ENSO. Their corresponding EOF patterns all display positive values over the WTP, Aqua/Terra MODIS and SeaWiFS EOFs also show negative values over the ETP (Figure 1). As the mean seasonal cycle, which explained most of the variability has been removed, this EOF explains $\sim 6\text{--}8\%$ of the remaining variance in all data sets. Because of the high spatial and temporal variability of aerosols owing to the nature of the aerosol sources and heterogeneity of the aerosol types, the variances explained by the leading EOFs (Figure 2) are in general lower than typical meteorological data sets. The different

behavior of MISR data over the ETP is because the dipole pattern has been split into two EOFs. The second EOF of MISR AE shows only negative values over the ETP and has a correlation coefficient with MEI of 0.44. We also investigated the lag correlation between the PCs and MEI and found the highest correlation occurs at zero lag across all data sets.

[17] Results of EOF analysis suggest a positive correlation between satellite-retrieved AE and ENSO over the WTP and a negative correlation over the ETP. We further examine the time evolution of the AE anomalies over the tropical Pacific region directly, having in mind that EOF analysis occasionally produces spurious correlations. Figure 3 shows the time versus longitude Hovmoller diagrams of monthly AE anomalies averaged between 10°S and 10°N . The MEI time series is superimposed to indicate El Niño and La Niña events. Hovmoller diagram of SST data is also shown as reference. In all four data sets, the AE over the WTP (mostly between 120°E and 180°E) has positive anomalies during El Niño, especially notable for the three strongest events in 2002, 2006 and 2009. Meanwhile, the AE anomalies over the ETP (140°W to 80°W) appear to be correlated with La Niña, with positive anomalies found during the major La Niña events of 2000–2001, 2005–2006, 2007–2008, and 2010–2011. The greatest increase (decrease) in the AE over the WTP (ETP) occurred during the strongest El Niño (La Niña) events of 2006 (2007). For the rest of the time, however, the magnitude of AE anomaly is not directly proportional to the strength of ENSO events; for example, positive AE anomaly over the WTP is greater during a weak El Niño in 2001 than during the strong El Niño in 2002. Moreover, despite agreeing on the major features, differences exist between the satellite data sets. Aqua and Terra MODIS data are consistent and have the most prominent ENSO signal. For MISR, the center of positive AE anomaly over the WTP during El Niño events is shifted about 20° westward relative to the MODIS data. Also, the positive AE anomaly over the ETP in the MISR data seems to lead the La Niña peak by about 3 months in late 2005 and 2007. The SeaWiFS data have similar patterns to the other data sets after removing an apparent linear trend. The differences in the details of the ENSO-AE relationship in the WTP and the ETP between different data sets are most likely attributed to differences in the space-time sampling of the satellite measurements. For example, the difference between MODIS and MISR results may arise from the much narrower swath width of the MISR instrument (360 km versus 2330 km for MODIS). Moreover, this smaller swath width results in a longer repeat time for MISR, which is 9 days at the equator, as compared to the 2 days for MODIS. The sampling strategy and repeat time for SeaWiFS is similar to those of MODIS. Nevertheless, this ENSO signal is robust in that it exists in all four data sets. In the following discussion, we will focus on MODIS AE data since it has the best correlation with ENSO.

[18] In order to further examine the AE-ENSO correlation, averaged MODIS AE anomaly time series from the two key regions in the WTP and ETP (two rectangles marked in Figure 1) are computed and compared with the MEI time series (Figure 4). Both time series are found to be correlated with the MEI, with higher correlations over the WTP. The correlation between their differences and the MEI

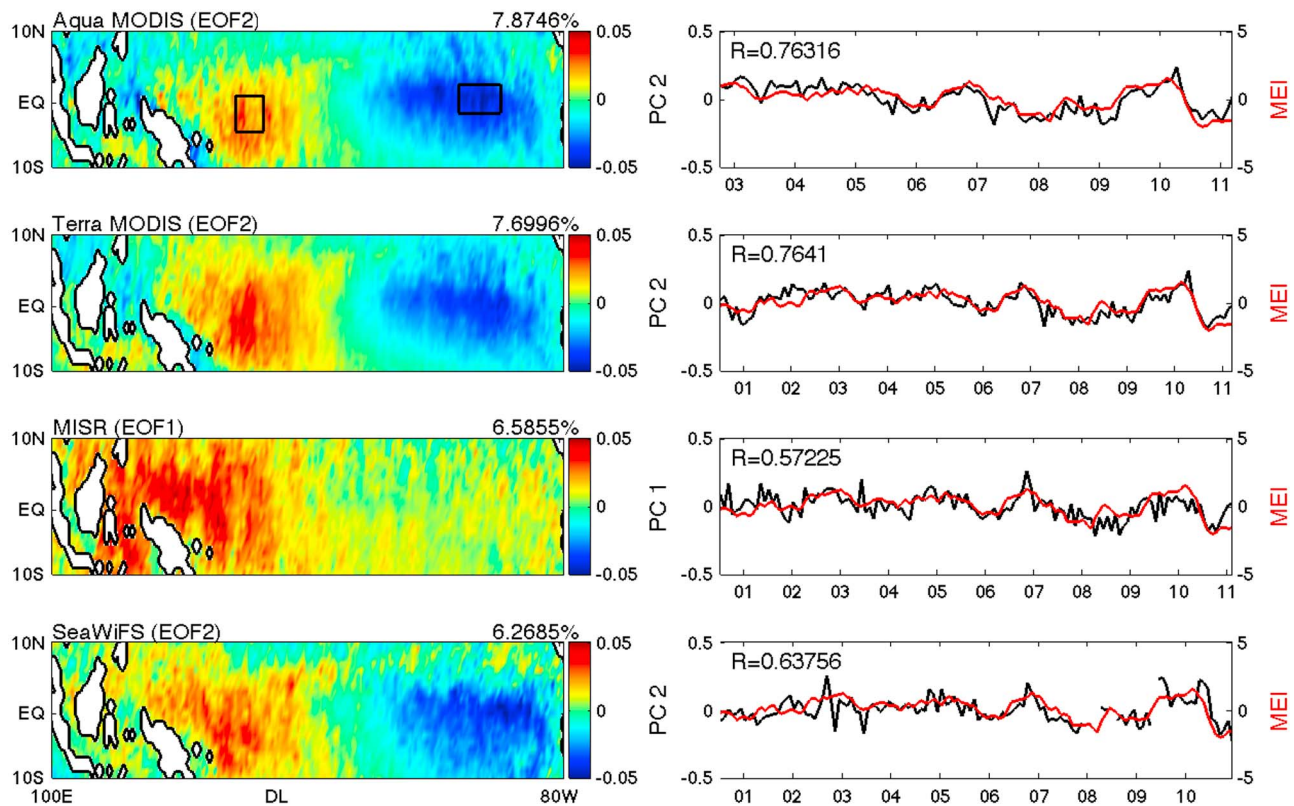


Figure 1. EOF analysis of the four AE data sets. The second EOF of Aqua, Terra MODIS, and SeaWiFS data; the first EOF of MISR data; and their corresponding PCs are correlated with ENSO. The lack of a dipole pattern in the MISR data is because the second EOF of this data set shows only the negative signal over the ETP. However, it is not included, as its correlation with ENSO (0.44) is lower than the first EOF (0.57). All correlation coefficients are computed at 95% confidence level. The number on the top right corner of each EOF panel is the percentage of variance explained by this EOF. The two boxes marked on the first panel indicate two key regions that are mostly influenced by the ENSO.

is significantly higher than that for the individual time series. Just like ENSO index which is defined as the sea surface temperature or pressure differences between the WTP and ETP, the difference between the AE anomaly over the WTP and ETP could also be considered as a type of ENSO index related to changes in aerosol properties over the tropical Pacific. This change could be due to aerosol compositional changes, size changes or other effects and will be discussed in section 4.

[19] Interestingly, it should be noted that despite coherent ENSO versus non-ENSO differences in AOD [e.g., *Tosca et al.*, 2009], EOF analysis of AOD data does not result in the isolation of an ENSO mode. Instead, the ENSO signal appears as an interannual modulation of the AOD variability. This might be attributed to the sensitivity of the AOD EOFs to space-time variations in aerosol source. Also, the correlation between the AOD time series and ENSO index is also below 0.5 over both the WTP and the ETP.

4. Discussion

[20] The above analysis reveals an evident and comparatively robust influence of ENSO on satellite-retrieved AE over the tropical Pacific. However, the direct link between ENSO and AE, and the physical processes that are respon-

sible for this phenomenon are still unclear. Although the change in AE is generally associated with changes in aerosol size distribution, the actual cause could be either a change in the actual size or a change in aerosol fine/coarse mode composition. Moreover, as aerosol-cloud cover correlations have been reported in the literature [*Kaufman et al.*, 2002, 2005; *Zhang et al.*, 2005; *Zhang and Reid*, 2006], this AE-ENSO correlation might also be the result of aerosol sampling changes or cloud contamination. Also, relative humidity altered by SST anomalies may affect the hygroscopic growth of some aerosol species. In addition, tropical ozone concentration and ocean color, which are also affected by ENSO, could potentially contaminate the AE data by affecting AOD retrievals at certain wavelengths. In this section, we examine the manner in which these mechanisms might contribute to the observed AE-ENSO relationship.

[21] We start by examining several key ENSO-related meteorological parameters and their correlation with the AE, including zonal wind, wind speed, relative humidity, precipitation and cloud fraction. Figure 5 shows the results of EOF analysis of these meteorological fields over the tropical Pacific. These EOFs are selected according to the criterion described at the beginning of section 3. All parameters show strong ENSO correlation. The PC of surface wind speed has the highest correlation with the PC of Terra MODIS AE,

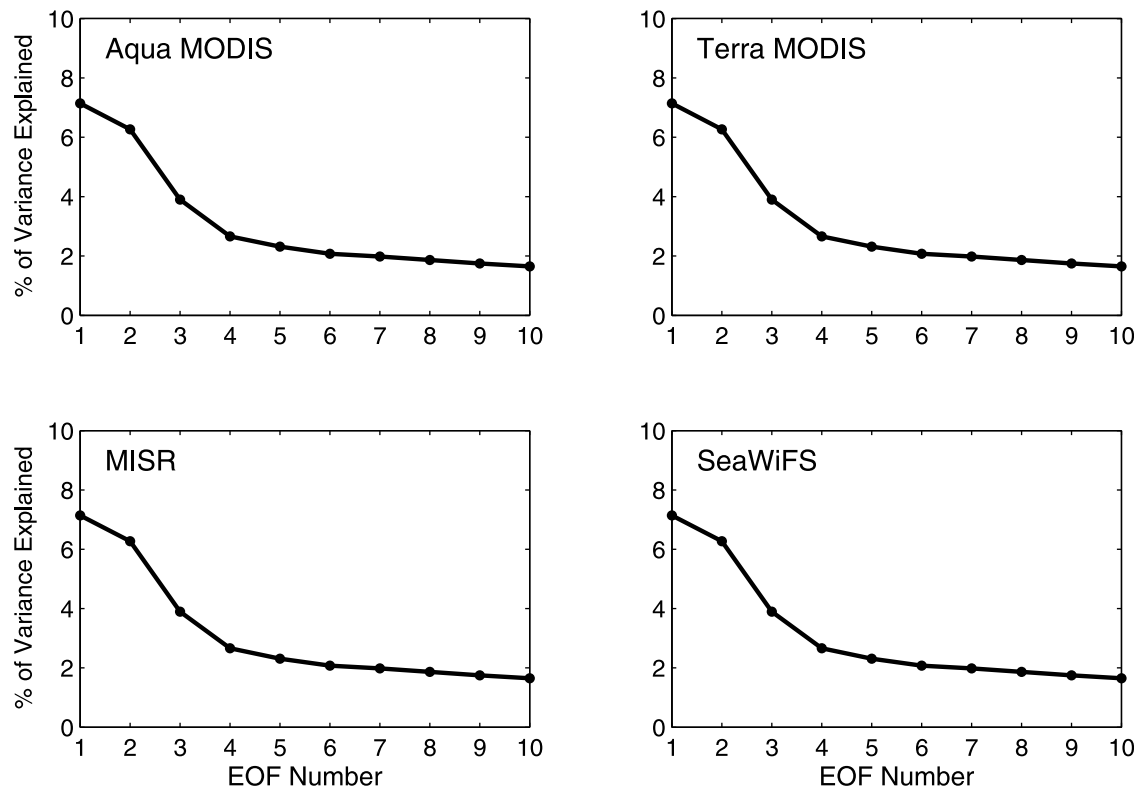


Figure 2. Percentage of variance explained by each EOF of the four AE data sets.

with precipitation and cloud fraction ranging second and third, and the lowest correlation is found between the AE and relative humidity. The dipole EOF pattern of wind speed, especially over the WTP, also closely resembles that of the AE. Precipitation and cloud fraction fields both show the positive anomaly over the WTP, consistent with the AE. However, they lack the negative anomaly over the ETP. The correlation between the anomaly time series over the two key regions (rectangles in the first panel of Figure 1) are consistent with EOF analysis (Figure 6), indicating highest correlation between wind speed and AE over the WTP. However, over the ETP, no meteorological parameter considered has significant correlation with the AE.

[22] The influences of wind speed on aerosol properties mainly come from two mechanisms: (1) affecting sea-salt production over the open sea surface and (2) affecting aerosol transport from their source regions. For the first factor, *Smirnov et al.* [2003] showed that sea-salt production is proportional to surface wind speed. During El Niño, the surface westward trade wind is suppressed (corresponding to a positive anomaly in the eastward zonal wind as appeared in the EOF), which reduces sea-salt concentration and has the effect of increasing AE by reducing coarse mode particles. For the second effect, ENSO events are associated with atmospheric circulation anomalies, when both surface westward wind and high-level eastward wind weakened and thus a weaker Walker circulation. This might alter aerosol transport from North and South America over lower levels and from Asia over higher altitudes. Meanwhile, increased fires associated with El Niño events are well documented

over the adjacent Indonesian region. In order to investigate aerosol transport pathways as well as its changes with ENSO, we use NOAA HYSPLIT model [*Drexler and Hess, 1998*] to calculate 7 day backward trajectories of air masses arriving at the two key regions. The results are summarized into four animations available in the auxiliary material.¹ The sources of air masses are identified by clustering the end points of each trajectory. It is found that: (1) air masses coming from Indonesian to the WTP only account for a very small fraction, indicating this is not a significant source region, and (2) while the transport pattern during El Niño and La Niña are slightly different, they both show that low-altitude air masses are mostly from sea surface for both regions. At higher altitudes, a small portion of air masses may carry Asian aerosols to the WTP, whereas for the ETP there seems to be no obvious land sources. As a result, we believe aerosol transport should play an unimportant role in the WTP. Furthermore, we use CALIPSO level 2 vertical feature mask product to examine aerosol compositional or mixing changes. Figure 7 shows the frequency distribution as a function of height for clean marine, polluted dust and undetermined aerosol types for the WTP and the ETP during ENSO and non-ENSO seasons. For the WTP (top), it is clear that the data clusters by ENSO phase with the El Niño years (2006 and 2009) have significant lower-frequency occurrence of marine aerosols than normal and La Niña years (2007, 2008 and 2010). As marine aerosols are

¹Auxiliary materials are available in the HTML. doi:10.1029/2011JD015733.

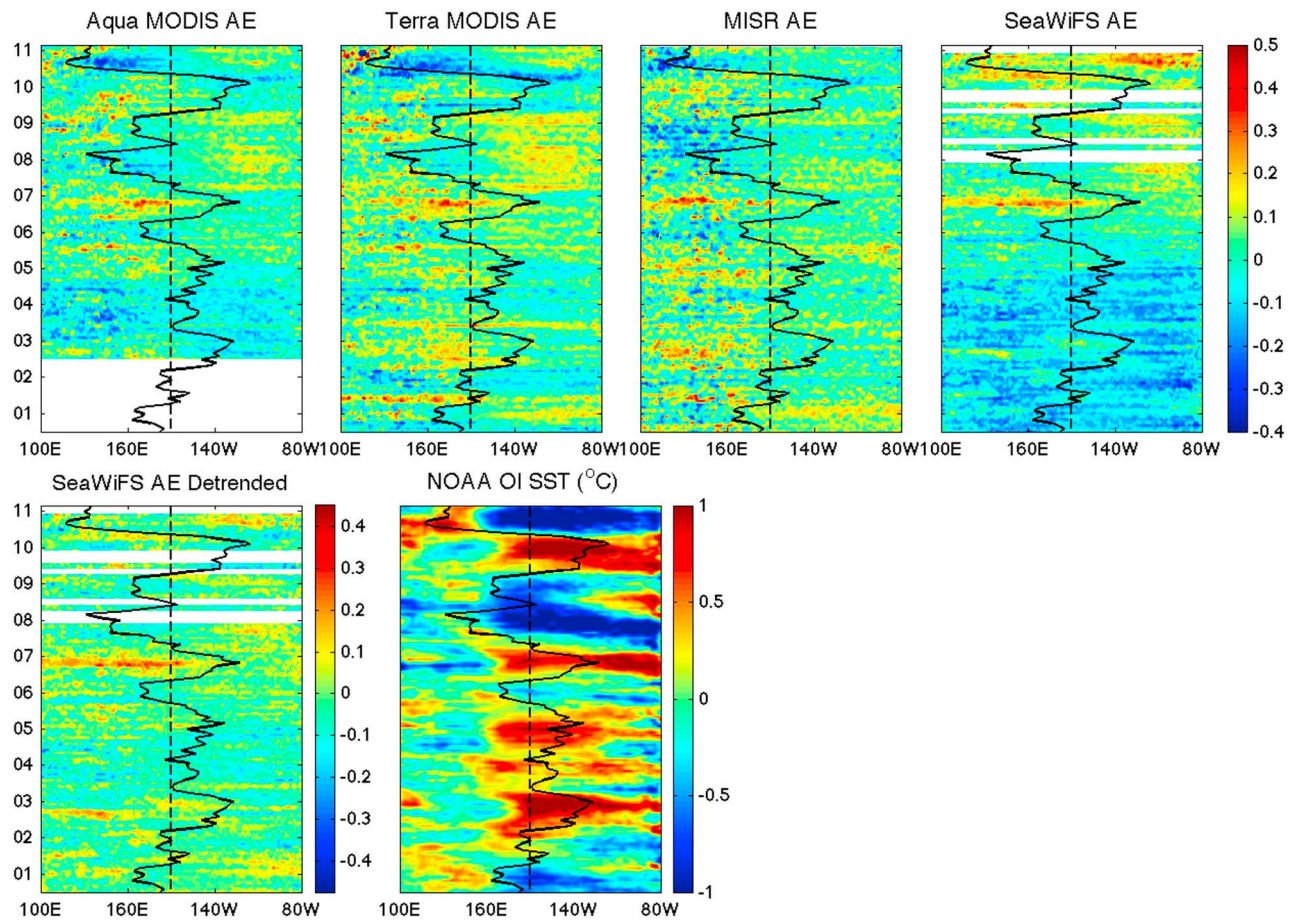


Figure 3. Time versus longitude Hovmoller diagram of monthly mean AE anomalies from four data sets averaged between 10°S and 10°N. MEI time series are superimposed (solid black lines) to indicate El Niño and La Niña events. The dashed black lines indicate the zero line for MEI. In all four data sets, positive AE anomaly appears over WTP during El Niño and over ETP during La Niña. A Hovmoller diagram of NOAA OI SST is also presented as reference.

primarily coarse mode, their reduction is likely responsible for the AE increase over the WTP. Moreover, the undetermined aerosol profiles have higher frequencies of occurrences during the same period, which also suggests a change in aerosol mixing. For the ETP, the most prominent feature is the appearance of a higher layer of polluted dust aerosols for the La Niña year of 2010. This may be associated with enhanced transport by the strengthened Walker circulation. In addition, the profile data suggest slightly lower frequency of sea-salt aerosol during La Niña and normal years than El Niño years, which is consistent with the weak wind speed increase (EOF1 from Figure 5) and AE decrease, although the contrast between El Niño and La Niña years is not as strong as in the WTP.

[23] In addition to the physical mechanism discussed above, wind speed also affects ocean surface roughness and whitecaps. However, this effect is not taken into account in the MODIS aerosol retrieval algorithm. Higher wind speed might whiten the surface, creating a flatter spectral reflectance and thus a smaller AE, and vice versa. Therefore, this effect also contributes to the correlation between AE and

ENSO and may partly explain why the highest correlation found in MODIS data.

[24] Cloud fraction is considered to be the second largest contributing factor to the observed AE changes. On the one hand, cloud contamination is the largest source of uncertainty in satellite retrievals of aerosol properties. On the other hand, the ENSO induced shift in cloud changes the distribution of clear-sky pixels from which the aerosol information is retrieved. Cloud contamination has been found to be responsible for many of the observed aerosol changes in remote sensing data. For example, *Tian et al.* [2008] attributed the observed correlation between satellite-retrieved aerosol properties and the MJO mainly to clouds. Here we suggest that cloud contamination should not be a factor, because both cloud fraction and cirrus reflectance increase over the same region as AE increases, and cloud contamination of the aerosol data would result in a smaller AE value contrary to the observations. Changes in aerosol sampling might also play a role, as the number of clear pixels that are used to retrieve aerosols is decreased at higher cloud fraction.

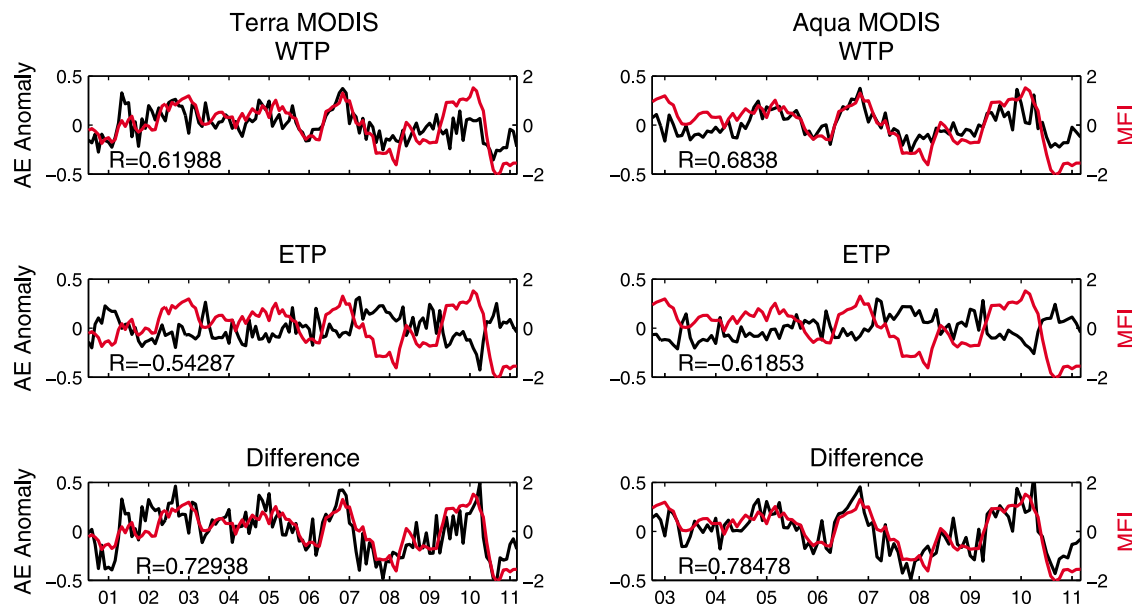


Figure 4. Correlation between ENSO and averaged MODIS AE anomaly time series for WTP, ETP, and their difference. The AE anomaly over the western Pacific has higher correlation with ENSO than with the eastern Pacific. The correlation between the difference of the two time series and ENSO is higher than their individuals and could be defined as another type of ENSO index.

[25] The third factor responsible for the AE-ENSO correlation is considered to be precipitation, which is very efficient in removing atmospheric aerosols through wet deposition. Also, near-surface, hygroscopic aerosols, such as sea salt, are more likely to be captured by rain [Tian *et al.*, 2008]. In the El Niño events, increased rainfall over the WTP as shown in the EOF tend to remove more sea-salt aerosols, which could also contribute to the observed CALIPSO aerosol type changes and has the effect of increasing the AE.

[26] We also take relative humidity effect into consideration, bearing in mind that relative humidity changes associated with SST anomalies will affect the hygroscopic growth of aerosols. However, this factor is also insignificant because relative humidity also increases over the region with positive AE anomaly. If it affects aerosol size, it will increase the size of hygroscopic aerosols and result in a decrease in the AE. Moreover, the correlation between the PCs and time series of relative humidity and AE are much lower compared with the first three parameters.

[27] In addition to meteorological fields, we also examine possible influence of tropospheric ozone concentration and ocean color variations, as these two quantities are also highly correlated with ENSO and might contaminate aerosol retrievals. Chandra *et al.* [2009b] found that tropospheric ozone increases over the WTP during El Niño due to increased biomass burning. However, the peak absorption by ozone in the Chappuis band is near 600 nm. If it affects aerosol measurements, it would result in a flatter optical depth spectral dependence thus smaller AE, opposite to what has been observed in the AE data. Surface chlorophyll concentration over the tropical Pacific is also found to vary with ENSO [Behrenfeld *et al.*, 2001], which alters ocean color and has the potential to affect aerosol retrievals. However, the correlation coefficient between the time series

of AE and chlorophyll concentration anomalies from both MODIS and SeaWiFS are low (<0.2 , figure not shown). Moreover, Siegel *et al.* [2000] showed that only very high chlorophyll concentration ($>2 \text{ mg m}^{-3}$) will result in an overestimate of satellite-retrieved AOD at visible wavelengths, while the value at both WTP and ETP are significantly lower than this threshold. These results suggest that ocean color is also unlikely to be a major factor.

[28] The above discussions suggest a clearer picture for the WTP: the highest correlation found between surface wind speed and the AE, supported by back trajectories and CALIPSO aerosol type profiles, suggests that aerosol changes during El Niño mainly arise from a local sea-salt reduction. Aerosol sampling changes associated with cloud shifts and wet removal by precipitation may also play important roles. Nonetheless, the exact physical process may be an interaction among these factors. For the ETP, the mechanism is unfortunately still obscure. It may involve complicated interaction between different processes, some of which may not have been considered. For example, some studies suggested possible correlation between aerosol properties and the QBO over the tropical Pacific [e.g., Dutton, 1991; Kane, 1994]. However, provided that satellite observations only became available in the past decade which has irregular ENSO cycles, the current record is too short to separate signals of different time scales, and to identify the source of the AE signal. Future research is still needed to find the causal relationship between the ENSO and AE over the ETP. Advanced remote sensing and in situ measurements, such as polarization remote sensing techniques and field campaign experiments, are likely required to solve this problem. Nonetheless, the CALIPSO data provides an indication of changes in the vertical distribution of aerosols with elevated aerosol layers more commonly associated with the La Niña.

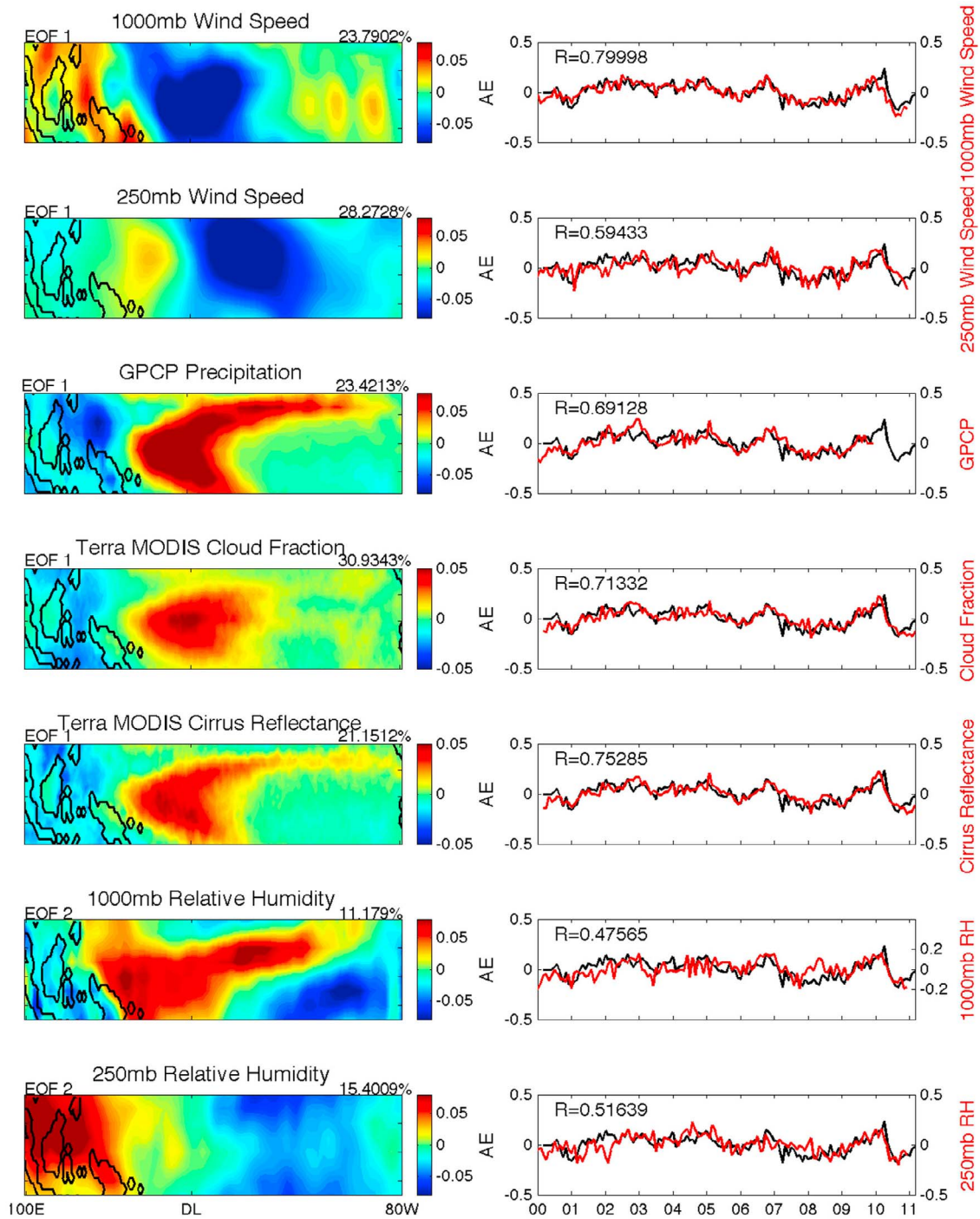


Figure 5. EOF analysis of key meteorological parameters, including zonal wind speed and relative humidity at the surface and 250 mb, precipitation, and cloud fraction. The first EOF of these meteorological parameters is highly correlated with ENSO. (right) The correlation between their principal components (PCs) and PC2 (second PC) of Terra MODIS AE is shown.

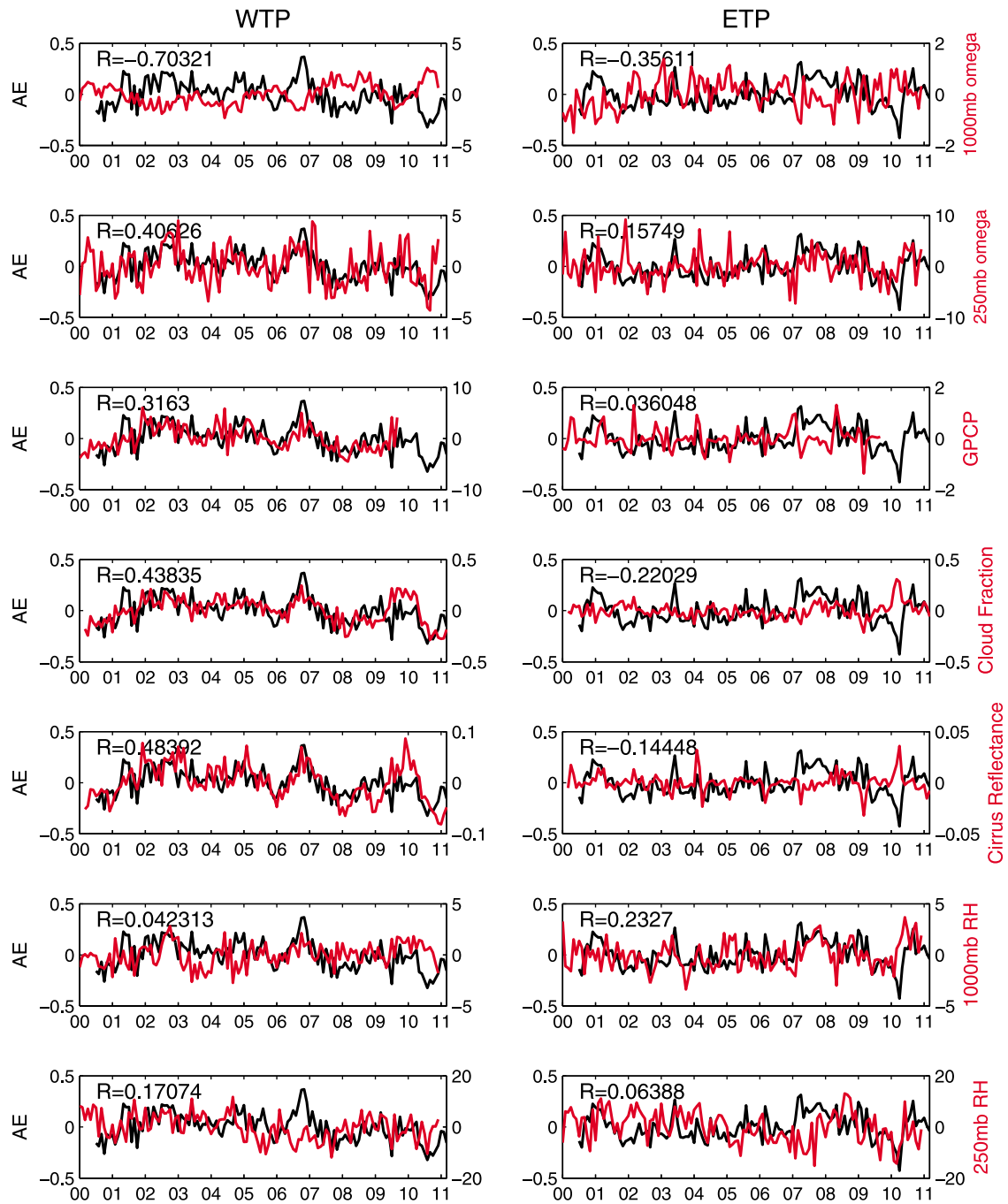


Figure 6. Correlation between the anomaly time series of AE and key meteorological parameters, including zonal wind speed and relative humidity at surface and 250 mb, precipitation, and cloud fraction.

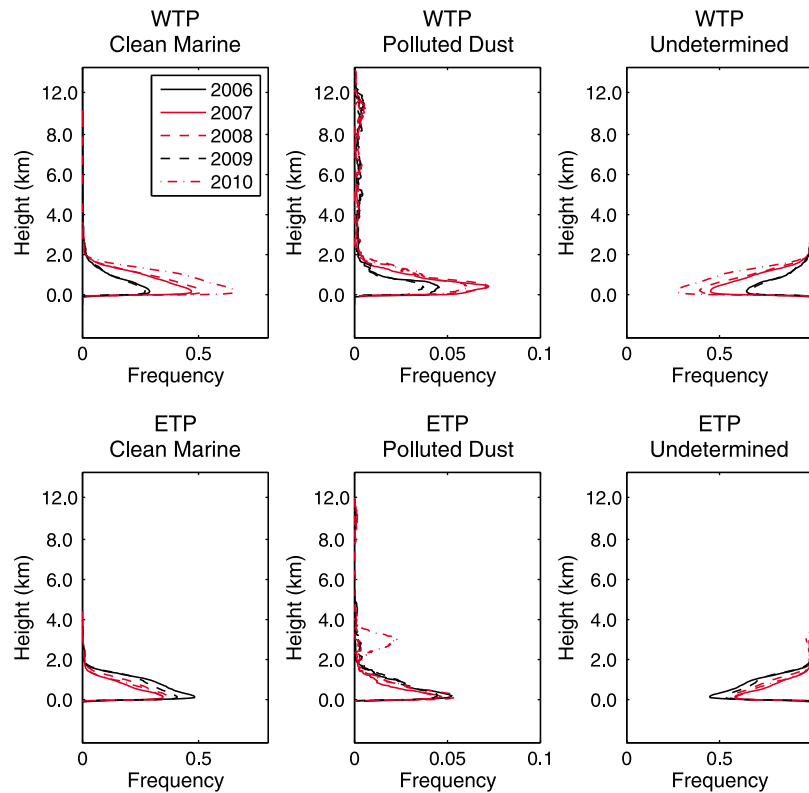


Figure 7. Frequency of appearance of CALIPSO profiles identified as two major aerosol types and an undetermined aerosol type over the WTP and ETP during the November to January period of 2006, 2007, 2008, 2009, and 2010. The frequency is calculated as the ratio of CALIPSO profiles identified as the specified aerosol type to the total number of profiles overpassing the region of interest during the 3 months. Over the WTP the frequencies of clean marine aerosols cluster by El Niño (2006, 2009) and non-El Niño periods, with lower frequency during El Niño. This phenomenon suggests a change in aerosol mixing over this region during ENSO, while the ETP has slightly higher marine aerosols during El Niño. Also, the elevated polluted dust layer during the strong 2010 La Niña suggests potential influence of aerosol transport.

[29] It should also be noted that as no significant signal is found in the AOD data, the AE anomaly is likely the result of changes in aerosol composition, while the AOD is sensitive to total aerosol loading. Advanced satellite and field campaign measurements are likely required to further examine the details of the change.

5. Summary and Conclusions

[30] In this study, we report an ENSO covariability in the AE parameter over the tropical Pacific present in four independent satellite data sets. EOF analysis, combined with Hovmöller diagrams of the AE anomalies over the tropical Pacific demonstrate a dipole pattern during El Niño, with positive values over the WTP and negative values over the ETP. Slight spatial-temporal shifts exist among the different data sets. The difference between the averaged time series of MODIS AE anomalies from two key regions (WTP and ETP) is highly correlated with MEI and could be considered as another type of ENSO index. However, no strong correlation has been found between AOD over the tropical Pacific and ENSO.

[31] Changes in several meteorological parameters, including wind speed, precipitation, relative humidity, cloud

fraction and cirrus reflectance, might be responsible for the AE variation observed during ENSO. By correlating their ENSO-related EOF patterns as well as time series with those of the AE, we identify surface wind speed anomaly as the primary cause for the WTP, through a reduction in sea-salt aerosol production. Cloud and rainfall might also play important roles through wet deposition of hygroscopic aerosols and changes in the distribution of clear pixels. Influences from relative humidity, tropospheric ozone concentration and surface chlorophyll concentration have been ruled out. The mechanism for the ETP may involve the interaction of multiple parameters as well as other climate modes and thus requires future research.

[32] Understanding this AE-ENSO relationship is important in studying the aerosol-ENSO interaction, aerosol indirect effect as aerosol size affects cloud formation and even ENSO prediction. However, the ENSO impact on aerosol size or composition may be due to a series of physical processes, some may not be among the above factors, or may be a complicated interaction between different factors. Further investigation is required to fully understand the details of the underlying mechanism(s). For example, the ongoing research on implementing polarization techniques in aerosol remote sensing will provide measurements of aerosol single

scattering albedo and refractive indices enhancing information on aerosol composition. Field campaign measurements of aerosol properties over the regions of interest, and model simulations of the ENSO-aerosol interactions will also be helpful in addressing this problem.

[33] **Acknowledgments.** We would like to thank the MODIS, MISR, and SeaWiFS instrument and algorithm teams for providing data used in this research. We also thank the Physical Sciences Division of the NOAA Earth System Research Laboratory for providing MEI data. NOAA_OI_SST_V2 data and NCEP Reanalysis 2 wind field and relative humidity data are provided by NOAA/OAR/ESRL PSD, Boulder, Colorado, USA. GPCP data are provided by the Mesoscale Atmospheric Processes Branch of the Laboratory for Atmospheres, NASA Goddard Space Flight Center. We would also like to thank the CALIPSO team for providing the vertical feature mask data set.

References

- Adler, R. F., et al. (2003), The Version 2 Global Precipitation Climatology Project (GPCP) monthly precipitation analysis (1979–present), *J. Hydro-meteorol.*, *4*, 1147–1167, doi:10.1175/1525-7541(2003)004<1147:TVGPCP>2.0.CO;2.
- Behrenfeld, M. J., et al. (2001), Biospheric primary production during an ENSO transition, *Science*, *291*, 2594–2597, doi:10.1126/science.1055071.
- Björnsson, H., and S. A. Venegas (1997), *A Manual for EOF and SVD Analysis of Climate Data*, CCGCR Rep. 97-1, 52 pp., McGill Univ., Montreal, Que., Canada.
- Chandra, S., J. R. Ziemke, J. R. Min, and W. G. Read (1998), Effects of 1997–1998 El Niño on tropospheric ozone and water vapor, *Geophys. Res. Lett.*, *25*, 3867–3870, doi:10.1029/98GL02695.
- Chandra, S., et al. (2009a), Tropical tropospheric ozone: Implications for dynamics and biomass burning, *Atmos. Chem. Phys.*, *9*, 4239–4249, doi:10.5194/acp-9-4239-2009.
- Chandra, S., J. R. Ziemke, B. N. Duncan, T. L. Diehl, N. J. Livesey, and L. Froidevaux (2009b), Effects of the 2006 El Niño on tropospheric ozone and carbon monoxide: Implications for dynamics and biomass burning, *Atmos. Chem. Phys.*, *9*, 4239–4249, doi:10.5194/acp-9-4239-2009.
- Diaz, H. F., M. P. Hoerling, and J. K. Eischeid (2001), ENSO variability, teleconnections and climate change, *Int. J. Climatol.*, *21*, 1845–1862, doi:10.1002/joc.631.
- Diner, D. J., et al. (1998), Multiangle Imaging Spectroradiometer (MISR) description and experiment overview, *IEEE Trans. Geosci. Remote Sens.*, *36*, 1072–1087, doi:10.1109/36.700992.
- Drexler, R. R., and G. D. Hess (1998), An overview of the HYSPLIT 4 modeling system for trajectories, dispersion and deposition, *Aust. Meteorol. Mag.*, *47*, 295–308.
- Dutton, E. G. (1991), A coherence between the QBO and the amplitude of the Mauna Loa atmospheric transmission annual cycle, *Int. J. Climatol.*, *12*, 383–396, doi:10.1002/joc.3370120406.
- Eck, T., B. N. Holben, J. Reid, O. Dubovik, A. Smirnov, N. O'Neill, I. Slutsker, and S. Kinne (1999), Wavelength dependence of the optical depth of biomass burning, urban, and desert dust aerosols, *J. Geophys. Res.*, *104*, 31,333–31,349, doi:10.1029/1999JD900923.
- Gong, S. L., X. Y. Zhang, T. L. Zhao, X. B. Zhang, L. A. Barrie, I. G. McKendry, and C. S. Zhao (2006), A simulated climatology of Asian dust aerosol and its trans-Pacific transport. Part II: Interannual variability and climate connections, *J. Clim.*, *19*, 104–122, doi:10.1175/JCLI3606.1.
- Gordon, H. R., and M. Wang (1994), Retrieval of water-leaving radiance and aerosol optical thickness over the oceans with SeaWiFS: A preliminary algorithm, *Appl. Opt.*, *33*, 443–452, doi:10.1364/AO.33.000443.
- Hooker, S. B., W. E. Esaias, G. C. Feldman, W. W. Gregg, and C. R. McClain (1992), An Overview of SeaWiFS and Ocean Color, *NASA Tech. Memo. TM-104566*, vol. 1, 65 pp.
- Kanamitsu, M., W. Ebisuzaki, J. Woollen, S.-K. Yang, J. J. Hnilo, M. Fiorino, and G. L. Potter (2002), NCEP-DEO AMIP-II Reanalysis (R-2), *Bull. Am. Meteorol. Soc.*, *83*, 1631–1643.
- Kane, R. P. (1994), Interannual variability of some trace elements and surface aerosol, *Int. J. Climatol.*, *14*, 691–704, doi:10.1002/joc.3370140608.
- Kaufman, Y. J., A. Gitelson, A. Karnieli, E. Ganor, R. Fraser, T. Nakajima, S. Mattoo, and B. N. Holben (1994), Size distribution and scattering phase function of aerosol particles retrieved from sky brightness measurements, *J. Geophys. Res.*, *99*, 10,341–10,356, doi:10.1029/94JD00229.
- Kaufman, Y. J., D. Tanré, L. Remer, E. Vermote, and B. N. Holben (1997), Operational remote sensing of tropospheric aerosols over the land from EOS-MODIS, *J. Geophys. Res.*, *102*, 17,051–17,067, doi:10.1029/96JD03988.
- Kaufman, Y. J., D. Tanré, B. N. Holben, S. Mattoo, L. A. Remer, T. F. Eck, J. Vaughan, and B. Chatenet (2002), Aerosol radiative impact on spectral solar flux at the surface, derived from principal-plane sky measurements, *J. Atmos. Sci.*, *59*, 635–646, doi:10.1175/1520-0469(2002)059<0635:AROSS>2.0.CO;2.
- Kaufman, Y. J., et al. (2005), A critical examination of the residual cloud contamination and diurnal sampling effects on MODIS estimates of aerosol over ocean, *IEEE Trans. Geosci. Remote Sens.*, *43*, 2886–2897, doi:10.1109/TGRS.2005.858430.
- Le Page, Y., J. M. C. Pereira, R. Trigo, C. da Camara, D. Oom, and B. Mota (2007), Global fire activity patterns (1996–2006) and climatic influence: An analysis using the World Fire Atlas, *Atmos. Chem. Phys. Disc.*, *7*, 17,299–17,338, doi:10.5194/acpd-7-17299-2007.
- Levy, R. C., L. A. Remer, J. V. Martins, Y. J. Kaufman, A. Plana-Fattori, J. Redemann, and B. Wenny (2005), Evaluation of the MODIS aerosol retrievals over ocean and land during CLAMS, *J. Atmos. Sci.*, *62*, 974–992, doi:10.1175/JAS3391.1.
- Levy, R. C., L. A. Remer, and O. Dubovik (2007a), Global aerosol optical properties and application to MODIS aerosol retrieval over land, *J. Geophys. Res.*, *112*, D13210, doi:10.1029/2006JD007815.
- Levy, R. C., L. A. Remer, S. Mattoo, E. Vermote, and Y. J. Kaufman (2007b), Second-generation algorithm for retrieving aerosol properties over land from MODIS spectral reflectance, *J. Geophys. Res.*, *112*, D13211, doi:10.1029/2006JD007811.
- Levy, R. C., L. A. Remer, R. G. Kleidman, S. Mattoo, C. Ichoku, R. Kahn, and T. F. Eck (2010), Global evaluation of the Collection 5 MODIS dark-target aerosol products over land, *Atmos. Chem. Phys.*, *10*, 10,399–10,420, doi:10.5194/acp-10-10399-2010.
- Logan, J. A., I. Megretskaja, R. Nassar, L. T. Murray, L. Zhang, K. W. Bowman, H. M. Worden, and M. Luo (2008), Effects of the 2006 El Niño on tropospheric composition as revealed by data from the Tropospheric Emission Spectrometer (TES), *Geophys. Res. Lett.*, *35*, L03816, doi:10.1029/2007GL031698.
- Martonchik, J. V., R. A. Kahn, and D. J. Diner (2009), Retrieval of aerosol properties over land using MISR observations, in *Satellite Aerosol Remote Sensing Over Land*, edited by A. A. Kokhanovsky and G. de Leeuw, pp. 267–293, Springer, Berlin, doi:10.1007/978-3-540-69397-0_9.
- Mitchell, R. M., S. K. Campbell, and Y. Qin (2009), Recent increase in aerosol loading over the Australian arid zone, *Atmos. Chem. Phys. Disc.*, *9*, 21,619–21,645, doi:10.5194/acpd-9-21619-2009.
- Podgorny, I. A., F. Li, and V. Ramanathan (2003), Large aerosol radiative forcing due to the 1997 Indonesian forest fire, *Geophys. Res. Lett.*, *30*(1), 1028, doi:10.1029/2002GL015979.
- Prospero, J. M., and P. J. Lamb (2003), African droughts and dust transport to the Caribbean: Climate change implications, *Science*, *302*, 1024–1027, doi:10.1126/science.1089915.
- Remer, L. A., et al. (2002), Validation of MODIS aerosol retrieval over ocean, *Geophys. Res. Lett.*, *29*(12), 8008, doi:10.1029/2001GL013204.
- Remer, L. A., et al. (2005), The MODIS algorithm, products and validation, *J. Atmos. Sci.*, *62*, 947–973, doi:10.1175/JAS3385.1.
- Remer, L. A., et al. (2008), Global aerosol climatology from the MODIS satellite sensors, *J. Geophys. Res.*, *113*, D14S07, doi:10.1029/2007JD009661.
- Reynolds, R. W., N. A. Rayner, T. M. Smith, D. C. Stokes, and W. Wang (2002), An improved in situ and satellite SST analysis for climate, *J. Clim.*, *15*, 1609–1625, doi:10.1175/1520-0442(2002)015<1609:AIISAS>2.0.CO;2.
- Siegel, D. A., M. Wang, S. Maritorena, and W. Robinson (2000), Atmospheric correction of satellite ocean color imagery: The black pixel assumption, *Appl. Opt.*, *39*, 3582–3591.
- Smirnov, A., B. N. Holben, T. F. Eck, O. Dubovik, and I. Slutsker (2003), Effect of wind speed on columnar aerosol optical properties at Midway Island, *J. Geophys. Res.*, *108*(D24), 4802, doi:10.1029/2003JD003879.
- Tanré, D., Y. J. Kaufman, M. Herman, and S. Mattoo (1997), Remote sensing of aerosol properties over oceans using the MODIS/EOS spectral radiances, *J. Geophys. Res.*, *102*, 16,971–16,988, doi:10.1029/96JD03437.
- Tian, B., D. E. Waliser, R. A. Kahn, Q. Li, Y. L. Yung, T. Tyrannowski, I. V. Geogdzhayev, M. I. Mishchenko, O. Torres, and A. Smirnov (2008), Does the Madden-Julian Oscillation influence aerosol variability?, *J. Geophys. Res.*, *113*, D12215, doi:10.1029/2007JD009372.
- Tosca, M. G., J. T. Randerson, C. S. Zender, M. G. Flanner, and P. J. Rasch (2009), Do biomass burning aerosols intensify drought in equatorial Asia during El Niño? *Atmos. Chem. Phys. Disc.*, *9*, 23,319–23,348, doi:10.5194/acpd-9-23319-2009.
- van der Werf, G. R., J. T. Randerson, L. Giglio, J. G. Collatz, P. Kasibhatla, and A. F. Arellano (2006), Interannual variability in global biomass burn-

- ing emissions from 1997 to 2004, *Atmos. Chem. Phys.*, 6, 3423–3441, doi:10.5194/acp-6-3423-2006.
- Wang, M. (2000), The SeaWiFS atmospheric correction algorithm updates, *NASA Tech. Memo. TM-2000-206892*, 57–63.
- Westphal, D., and O. Toon (1991), Simulations of microphysical, radiative, and dynamical processes in a continental-scale forest fire smoke plume, *J. Geophys. Res.*, 96, 22,379–22,400, doi:10.1029/91JD01956.
- Zhang, J., and J. S. Reid (2006), MODIS aerosol product analysis for data assimilation: Assessment of over-ocean level 2 aerosol optical thickness retrievals, *J. Geophys. Res.*, 111, D22207, doi:10.1029/2005JD006898.
- Zhang, J., J. S. Reid, and B. N. Holben (2005), An analysis of potential cloud artifacts in MODIS over ocean aerosol optical thickness products, *Geophys. Res. Lett.*, 32(15), L15803, doi:10.1029/2005GL023254.
- Ziemke, J. R., and S. Chandra (2003), La Niña and El Niño-induced variabilities of ozone in the tropical lower atmosphere during 1970–2001, *Geophys. Res. Lett.*, 30(3), 1142, doi:10.1029/2002GL016387.
-
- B. E. Carlson, Department of Earth and Environmental Sciences, Columbia University, 2960 Broadway, New York, NY 10027, USA.
A. A. Lacis and J. Li, NASA Goddard Institute for Space Studies, 2880 Broadway, New York, NY 10025, USA. (jli@giss.nasa.gov)